Contents

1 The structure of particle-hardened alloys

1.1 Dispersed phases present in metals

In most theoretical discussions of strengthening mechanisms in particle-hardened alloys, attention is usually confined to the interaction of glide dislocations with finely-dispersed precipitates typically 10 nm in size. In real alloys of this type, however, dispersions of coarser particles also exist, which may play an important role in the deformation behaviour and particularly in the fracture behaviour of the alloy. The types of dispersed phases that may be present can be conveniently classified into three families.

1.1.1 Hardening precipitates

These may range in size from, say, 1 to 100 nm. Chapters 1 and 2 are particularly concerned with the formation of such dispersions and their effect upon the yield and work-hardening behaviour of the alloy. In steels and in age-hardening non-ferrous alloys the particles are formed by precipitation from supersaturated solid solution, and this constitutes by far the most commonly used technique in use for producing a dispersed second phase. Other methods include diffusion reaction techniques, such as nitriding of steel or internal oxidation of, for example, copper alloys, and powder-metallurgical techniques.

Internal oxidation has been used fairly extensively in academic studies to produce single crystals containing fine dispersions of oxide particles, which form admirable 'model' systems for basic study. An alloy suitable for this treatment consists of a dilute solid solution of a base metal in a more noble metal. When the alloy is heated under oxidizing conditions, oxygen diffuses into the alloy, producing a dispersion of the oxide of the base metal in a matrix of the noble metal. Typical alloys appropriate for this treatment would be copper containing, say 0.1wt% of silicon, aluminium or beryllium which form dispersions of SiO_2, Al_2O_3 and BeO respectively. These phases will have high thermodynamic stability in comparison with phases produced by precipitation from supersaturated solid solution, yet are more finely divided than is normally achieved by employing powder-metallurgical techniques of physically mixing powdered metals and oxides to produce composites.

Physical mixing of metal/oxide composites followed by compaction and sintering does not in general lead to the formation of structures

consisting of uniform dispersions of finely-divided oxide particles. Even if the oxides are evenly distributed (a state extremely difficult, if not impossible, to achieve by mixing methods) the minimum interparticle spacing could never be less than that of the metal powder granule size itself. Since the enhancement of properties by dispersions increases with decrease of the interparticle spacing, this size effect is a severe limitation to the utility of 'straight' powder-metallurgical methods in producing dispersion-hardened metal refractory systems.

One of the successful powder-metallurgical products in this field is the material known as SAP (sintered aluminium powder). This is made by the hot compaction of flake-shaped aluminium powder (of flake thicknesses in the range 0.01 to 0.1 μm) which contains up to about 15wt% alumina formed during the manufacture of the powder. The sintered products consist of a dispersion of alumina in aluminium, and they possess exceptional strength and thermal stability. The success of SAP arises from the extremely small aluminium-flake thickness, which provides the required small oxide-oxide distance in the product. Nickel-based alloys containing dispersed oxides such as ThO_2 (TD-Nickel and TD-Nichrome) have been successfully produced by precipitating a hydrous, oxygen-containing compound of the matrix metal on to dispersoid particles in the form of a colloidal aquasol. This is followed by reduction, compaction, sintering and densification which produces structures containing good dispersions of fine oxide particles.

1.1.2 Coarse residual particles

When considering such particles, which are larger than 1 μm in size, it is convenient to discuss separately the occurrence of these coarse inclusions in *steels* and those encountered in *non-ferrous alloys*.

Inclusions in steels

The origin and constitution of non-metallic inclusions in steels have been the subject of intense study over many years, as it has long been recognized that they are a potential source of weakness. It is for this reason that strenuous efforts are now made in the production of 'clean' steels for many applications. The three main sources of non-metallic inclusions are:

(i) deoxidation, and the segregation of the products of deoxidation;

(ii) the presence of sulphur and phosphorous, and the segregation of their compounds;

(iii) extraneous sources, including the trapping of slag and eroded refractory materials within the molten steel.

Considerable attention has been paid to the deformability of different types of non-metallic inclusions during hot-working. Silicate inclusions are

known to deform extensively above about 1000 °C, but below this temperature they either deform little or shatter and disperse, as do the higher-melting-point oxide inclusions. The other major inclusion-type is manganese sulphide, which is always present to some degree to 'tie up' the residual sulphur present in the steel which would otherwise be present as a low-melting-point FeS eutectic phase. The deformability of MnS increases relative to that of steel with decreasing rolling temperature of the steel. Very elongated stringers of MnS are encountered in wrought steels, and together with the silicate inclusions are usually considered to be the major cause of poor ductility.

Non-ferrous alloys

Coarse insoluble particles are formed during casting of non-ferrous alloys, and although these may be broken up and distributed more uniformly through the structure by hot-working of the ingot, they are again recognized as a potential source of weakness in the material. Commercial *aluminium alloys* contain from about 1% to 5% by volume of large iron- or silicon-rich inclusions, and may also contain copper-bearing particles arising from non-equilibrium microsegregation during solidification. Iron is, of course, the principal impurity in bauxite, so that its presence is not unexpected in the final product.

1.1.3 Intermediate-sized dispersoids

These may range in size from, say 0.1 to 1 μm, and we will again take as our example aluminium alloys (in which such particles are commonly found), although they may occur in many materials. Chromium, zirconium, or manganese is added to many commercial wrought aluminium alloys. The element usually remains in solution during casting, but during fabrication these alloys are normally given a so-called 'homogenization' heat-treatment at relatively high temperature. The heat-treatment results in the formation of precipitates of intermetallic compounds containing chromium, zirconium or manganese, whose size and spacing depend upon the temperature and time of homogenization. An example of such a dispersion in an Al-Mg-Si alloy is shown in fig. 1.1.

These dispersions have pronounced retardation effects upon the response of the alloy to recrystallization and grain growth, and are also known in some alloy systems to reduce the tendency for intergranular embrittlement in the fully-aged condition. We will return later to a consideration of their effect upon deformation and fracture processes in age-hardenable alloys.

It is clear, therefore, that in industrial alloys of practical significance, several families of precipitates of differing ranges of particle size are likely to be present and to have an effect upon the deformation and/or fracture

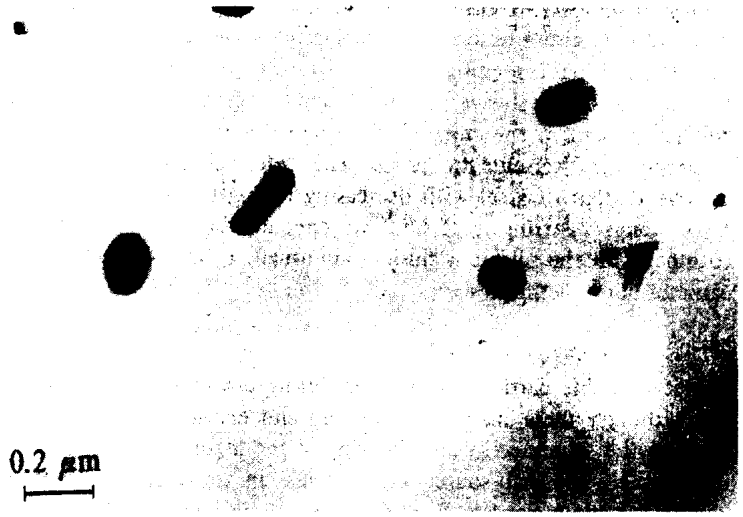

Fig. 1.1. Electron micrograph of an Al–0.6wt% Mg–1wt% Si–0.6wt% Mn alloy aged to peak hardness. The Mg_2Si phase is present as noncoherent particles at the grain boundaries and as the fine, coherent hardening phase within the grains. Note the narrow precipitate-free zone adjacent to the grain boundary. The Mn is present as dispersoids of the α-$Al_{12}Mn_3Si$ phase, typically 0.1 μm in size. (Courtesy of K. C. Prince.)

behaviour of the material. We will next consider the kinetics of the nucleation and growth of precipitates in solids, how such precipitates are distributed in the microstructure, and examine ways in which this distribution may be controlled.

This chapter will conclude with a consideration of how the distribution of precipitates in alloys may be quantitatively defined.

1.2 Precipitation in solids

Christian (1975) has reviewed the subject of precipitation in solids comprehensively, and this topic is dealt with at an introductory level in standard undergraduate texts on phase transformations in condensed systems. We will adopt a generalized mechanistic approach to account for the microstructures observed in metallic systems containing precipitates.

The decomposition of a phase into one or more phases may be divided into three stages: (i) the formation of nuclei of the new phase; (ii) the growth of these nuclei; and (iii) the coarsening of the precipitate without change in its volume fraction. Stage (i) may itself occur in two ways: if small concentration fluctuations may occur spontaneously, the reaction may proceed by *spinodal decomposition*; if all small fluctuations tend to

decay, there is said to be a nucleation barrier, and we will consider first the energy relations which contribute to the magnitude of this barrier, and then the kinetic factors which determine the rate at which the barrier is overcome and successful nucleation occurs.

1.2.1 Nucleation from supersaturated solid solution

Energy relations

We will initially consider a situation involving the homogeneous nucleation of a second phase, i.e. nucleation which occurs without the benefit of pre-existing heterogeneities in the system. The basic ideas of nucleation theory were originally expressed by Gibbs (1878), namely that work is necessary for the formation of the *surface* of a new phase.

Let us assume that, in a metastable α-phase, a β-region forms consisting of n atoms. If σ is the specific surface energy of the $\beta\alpha$ interface and Δg_c the specific chemical free energy of the β-phase, the balance of surface energy ($a\sigma n^{\frac{2}{3}}$) and the chemical energy due to the transformation in the new structure ($\Delta g_c\, nV$) is

$$\Delta G = a\sigma n^{\frac{2}{3}} + \Delta g_c\, nV,$$

where V is the atomic volume, and a depends upon the shape of the β-region, which in the simplest case is a sphere. Transformations in the solid state are also usually associated with a change in specific volume, which leads to distortions during nucleation. An elastic strain-energy term (g_e) should thus be included in the energy balance to give

$$\Delta G = a\sigma n^{\frac{2}{3}} + (\Delta g_c + g_e)\, nV. \tag{1.1}$$

The variation in ΔG with n will therefore be of the form shown in fig. 1.2 and the condition for continued growth of an embyro is that the

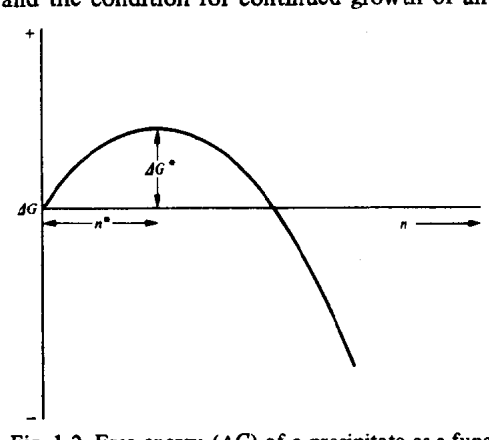

Fig. 1.2. Free energy (ΔG) of a precipitate as a function of the number of atoms it contains (n).

number of atoms it contains should exceed n^*, where $d\Delta G/dn = 0$, i.e.

$$n^* = \left(\frac{2a\sigma}{-3V(\Delta g_c + g_e)}\right)^3. \tag{1.2}$$

The critical free energy, or activation energy for nucleation, is given by

$$\Delta G^* = \tfrac{1}{3}\sigma n^{*\frac{2}{3}}. \tag{1.3}$$

For a spherical nucleus of radius r, the surface area is given by $4\pi r^2 = an^{\frac{2}{3}}$. Since $n = 4\pi r^3/3V$, we may substitute in equations (1.2) and (1.3) to obtain

$$r^* = \frac{2\sigma}{-(\Delta g_c + g_e)} \tag{1.4}$$

and

$$\Delta G^* = \frac{16\pi\sigma^3}{3(\Delta g_c + g_e)^2}. \tag{1.5}$$

Below the equilibrium temperature Δg_c becomes negative and increases roughly linearly with increasing undercooling (ΔT). The values of σ and g_e are assumed to be independent of temperature.

The temperature dependence of r^* and ΔG^* may be assessed in terms of the temperature dependence of Δg_c, so we can write as a first approximation

$$r^* \propto 1/\Delta T, \quad \Delta G^* \propto 1/\Delta T^2. \tag{1.6}$$

Basic kinetic theory

A steady-state nucleation rate, $\dot{N}_V$, may be defined as the number of stable nuclei produced in unit time in unit volume of untransformed solid. The theory assumes that the atomic fluctuations which give rise to the embryos are present in statistical equilibrium, so that if the number of atoms, n, in these fluctuations is much smaller than the total number of atoms, n_0, it follows from (1.1) that

$$n = n_0 \exp(-\Delta G/kT),$$

where k is the Boltzmann constant and T the absolute temperature. An embryo which contains a larger number of atoms than n^* (fig. 1.2) can grow with decreasing free energy and is called a nucleus, and it follows that the nucleation rate $\dot{N}_V$ is proportional to $\exp(-\Delta G^*/kT)$. The rate at which individual nuclei grow will also be dependent on the frequency with which atoms adjacent to the nucleus can join it, and this will be proportional to the volume diffusivity, D. One may therefore write a

simplified representation of the rate of nucleation of a precipitate

$$\dot{N}_V = KD \exp \frac{-A\sigma^3/(\Delta g_c + g_e)^2}{kT}, \tag{1.7}$$

where A is a geometrical constant and K another constant.

This relationship accounts for the observed minima in the incubation time in temperature-time-transformation (TTT) curves. Because of the high value of the energy of activation for diffusion (1 to 4 eV for substitutional atoms) the value of D, and thus the rate of nucleation becomes very low at low temperatures. At temperatures close to equilibrium, $\dot{N}_V$ becomes low because $\Delta G^* \to \infty$ (since $\Delta g_c \to 0$).

The precipitation of face-centred cubic (fcc) cobalt from fcc copper-cobalt alloys is one of the few systems which decompose by homogeneous nucleation. Servi & Turnbull (1966) have studied this system, and found that the theory predicts the temperature (at fixed composition, or vice-versa) for a given nucleation rate very accurately. In (1.7), g_e is neglected and Δg_c is taken as the product of kT and the natural log of the supersaturation, i.e. $kT \ln c/c_e$, where c is the cobalt content of a particular (supersaturated) alloy and c_e the equilibrium solubility of cobalt at the precipitation temperature. Servi & Turnbull presented their data in an activation plot. This plot is reproduced as fig. 1.3. The effective nucleation time is denoted by $\bar{t}$, so N_p (number of particles) divided by $\bar{t}$ is nucleation rate, and the plot shown in fig. 1.3 is arrived at by rearranging (1.7) and substituting for Δg_c. If σ is independent of temperature the plot should give a straight line, and Servi & Turnbull drew a straight line through their data

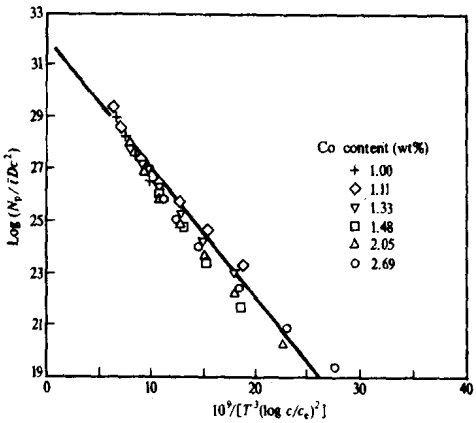

Fig. 1.3. Activation plot of data relating to the coherent nucleation of Co from a dilute solution of Co in Cu. (After Servi & Turnbull, 1966.)

and compared the slope and intercept to predictions of nucleation theory. The slope of fig. 1.3 corresponds to a value of σ of 0.23 J m^{-2}, which agrees well with a calculated value of 0.20 J m^{-2}, but the intercept on the vertical axis (corresponding to the pre-exponential term in (1.7)) of 32 is less than the anticipated value of 36, which may be due to experimental uncertainties and/or a curvature in the plot due to ignored surface entropy effects.

The behaviour of the Cu-Co system is not typical of most precipitated alloys of practical interest. Instead of the homogeneous nucleation of an equilibrium phase, metastable phases are commonly observed, and furthermore nucleation sites are very commonly associated with lattice defects in the matrix - in other words, one usually encounters *heterogeneous nucleation.*

1.2.2 Heterogeneous nucleation

In supersaturated solid solutions the following types of lattice defects can be expected;

0-dimensional faults - vacancies and interstitialcies;

1-dimensional faults - dislocations;

2-dimensional faults - grain and twin boundaries, stacking faults, anti-phase domain boundaries, and possibly interphase boundaries.

The rate of heterogeneous nucleation is again proportional to exp $(-\Delta G^*/kT)$ and the magnitude of ΔG^* is lower for the heterogeneous nucleation than for homogeneous nucleation due to the reduction in one or both of σ and g_e (1.1) caused by the interaction of the defects and the critical nucleus.

The crystal structures of the matrix and the precipitate must also be considered, because quite different structures and hence energies of the interface will arise from this factor. There are three important cases to define.

(i) *Coherent nucleation*: if the crystal structures and lattice parameters of both phases are closely similar, this will occur (fig. 1.4*a*). The precipitation of the Ni_3Al-phase in Ni is of this type, the dispersed particles being in parallel crystallographic orientation with the matrix.

(ii) *Semicoherent nucleation* arises if the α- and β-phases are related in such a way that an interface can be built from well-defined defects, such as interfacial dislocations (fig. 1.4*b*). The θ'-phase in the Al-Cu system is a familiar example of this type.

(iii) *Noncoherent nucleation* arises if the structures of the α- and β-phases are so different that the interface has a structure similar to that of a high-angle grain boundary (fig. 1.4*c*). The θ-phase in the Al-Cu system is of this type.

There is a limited number of fixed orientations between the α- and

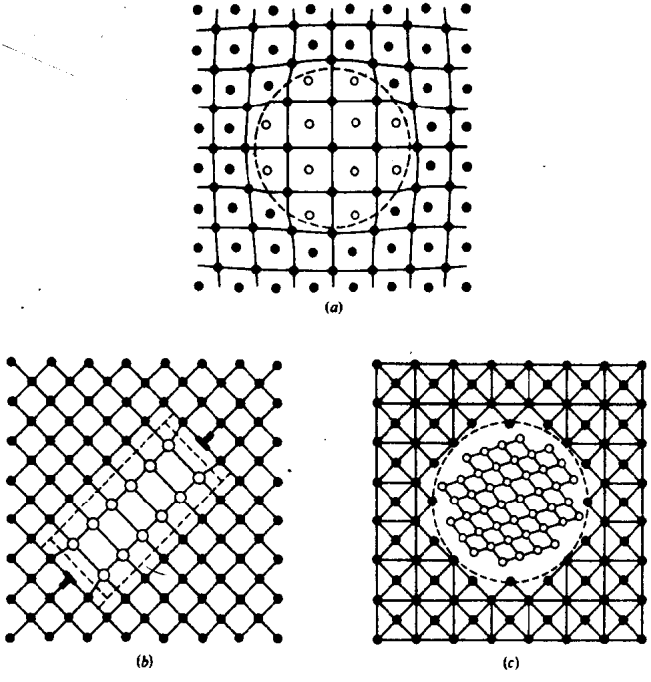

Fig. 1.4. (*a*) Fully coherent precipitate showing coherency strains in matrix. (*b*) Partially coherent precipitate showing interface dislocations. (*c*) Non-coherent precipitate.

β-phases which will allow coherent or semicoherent nucleation. In non-coherent nucleation, however, a random orientation between the two phases can be expected.

Heterogeneous nucleation on point defects

Quenched-in vacancies can affect the rate of precipitate nucleation in two ways. Firstly, they can increase the diffusion rate of solute atoms and thereby increase the growth rate of precipitate embryos. Secondly, vacancies may become an integral part of the nucleus and thereby reduce the nucleation barrier to precipitate formation. It is this latter function we will consider further for the moment. The nucleation of a misfitting precipitate will be facilitated if a number of vacancies accumulate in order to counteract the volume change, thus reducing g_e (see (1.1)). For strain-free nucleation (i.e. $g_e = 0$) the nucleus requires ρ_0 vacancies per atom, ρ_0 is given by

$$\rho_0 = \frac{V^\beta - V^\alpha}{V^\alpha},$$

where V^β is the atomic volume of the precipitate and V^α that of the matrix. Thus, in the presence of vacancies, the strain-energy may be written as $g'_e = g_e\,(1 - \rho/\rho_0)$, and the energy barrier to nucleation (1.5) now becomes

$$G^* = \frac{16\pi\sigma^3}{3[\Delta g_c + \Delta g_v + g_e\,(1 - \rho/\rho_0)]^2},$$

where Δg_v is the change in free energy associated with vacancy precipitation.

There is convincing scientific evidence that excess vacancy concentrations influence precipitation processes. Shepherd (1969) has, for example, shown that a much finer dispersion of carbide precipitates is formed in an irradiated stainless steel specimen than in an equivalent control specimen.

Excess point defects can of course condense to form small dislocation loops, or stacking-fault tetrahedra (depending on the material), and the possibility cannot be discounted that the nucleating sites in irradiated specimens are in fact vacancy aggregates of this type.

Heterogeneous nucleation on dislocations

The first theoretical model for nucleation on dislocations was due to Cahn (1957), who considered a cylindrical nucleus and allowed its misfit to balance the strain-energy of the dislocation so that g_e (1.1) is reduced and $\dot{N}_V$ is increased (1.7). Cahn expresses his result in terms of a dimensionless parameter.

$$\alpha = \frac{\Delta g_c\, Gb^2}{2\pi^2\sigma^2},$$

where G is the shear modulus and b the Burgers vector, and he showed that the effectiveness of dislocations to lower ΔG^* increases with increasing values of α. According to this model, therefore, dislocations with a large Burgers vector are more effective than those with a small one. Experimental investigations have indicated that the mechanism assumed as a basis for this theory is not observed very frequently: it is most realistic in dealing with particles with a spherically symmetrical strain field, such as Co in Cu-Co.

Hornbogen & Roth (1967) made a systematic study of the influence of Δg_e on nucleation in the matrix and on dislocations, by comparing the precipitation kinetics of alloys of comparable supersaturation (i.e. Δg_c = constant) but of varying lattice misfit strain (ϵ) associated with the precipitate. It was always found that the larger the value of ϵ, the larger the time gap between the beginning of nucleation at dislocations and in the matrix (fig. 1.5).

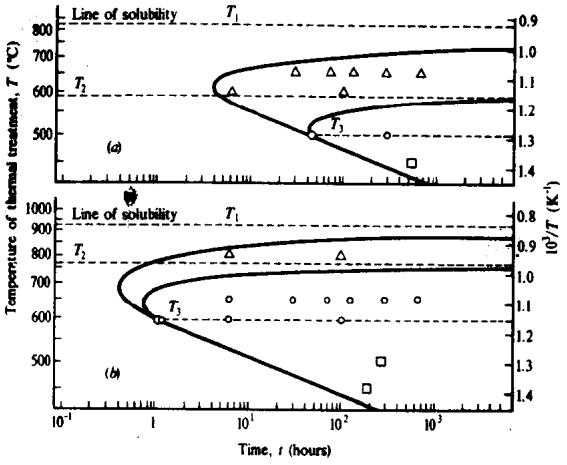

Fig. 1.5. Nucleation diagrams for precipitation in: (*a*) Ni–6.36wt% Al, misfit strain 0.4%; and (*b*) Ni–6.32wt% Al, misfit strain 0.34%. T_1 is the equilibrium temperature, T_2 is the temperature above which only dislocation nucleation takes place and T_3 is the temperature below which there is simultaneous nucleation at dislocations and in the matrix. (After Hornbogen & Roth, 1967.)

The greatest effectiveness of a dislocation in lowering the strain-energy and therefore the activation energy of nucleation is to be expected if the nucleus can be formed by dissociation of the dislocation into two partial dislocations. The nucleation event is then involved with a two-dimensional feature (the stacking-fault) rather than the one-dimensional dislocation, and we will discuss this further in § 1.2.3.

Precipitation on dislocations can lead to high precipitate densities if an autocatalytic process operates. For example when carbides of the type $M_{23}C_6$ precipitate in certain austenitic stainless steels the particles are found to lie in strings along ⟨110⟩ matrix directions. Studies of the early stages of ageing have shown that discrete particles are nucleated on the existing dislocations, and they grow partially coherently with the matrix. In order to accommodate the strains resulting from the difference in atomic volume between the two lattices, prismatic loops of dislocation are 'punched' out by the growing particle into the matrix (fig. 1.6). These punched loops (which have ⟨110⟩ glide axes) then act as sites for further precipitation of carbide, resulting in the formation of the stringers observed after long ageing times.

Still higher precipitate densities may also be achieved by introducing a high dislocation density into the supersaturated solid solution. These higher densities may arise through transformation strain, as in the case of marageing steels, in which martensite of high dislocation density is formed

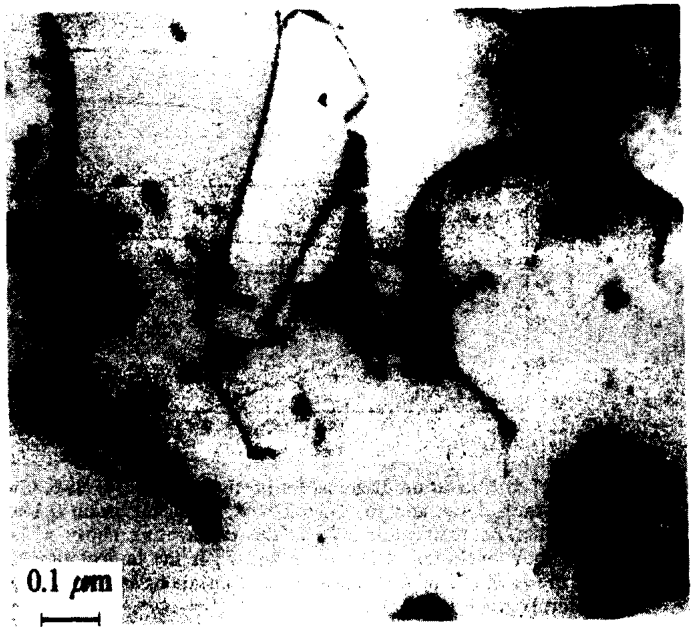

Fig. 1.6. Electron micrograph of precipitation of iron–chromium carbide ($M_{23}C_6$) in an austenitic stainless steel after ageing for 5.5 hours at 750 °C. Prismatic dislocation loops are being punched out into the matrix by the growing particles. (Courtesy of M. H. Lewis & B. Hattersley.)

on cooling, or through mechanical working, as in ausforming and other thermomechanical treatment. We will discuss these possibilities in §§ 1.3.3 and 2.4.4.

Heterogeneous nucleation on planar defects

Grain boundaries are effective in increasing $\dot{N}$, the rate of nucleation since, when a precipitate nucleus is formed in a boundary, part of the boundary area is eliminated and this energy is available effectively to reduce the σ-term in (1.7). The energy of a phase boundary is composed of two parts: (i) energy arising from the *structure* of the interface; and (ii) the *chemical* energy due to the difference in composition and order on both sides of the interface. Term (ii) leads to a difference between $\sigma_{\alpha\beta}$ and $\sigma_{\alpha\alpha}$ for an identical structure of grain boundary ($\alpha\alpha$) and phase boundary ($\alpha\beta$). Fig. 1.7 illustrates the form of a β-phase nucleus at an α-grain boundary, which for isotropic surface energies is in the form of a doubly spherical lens. The ratio of the specific surface energies is

$$\sigma_{\alpha\alpha}/2\sigma_{\alpha\beta} = \cos\tfrac{1}{2}\theta.$$

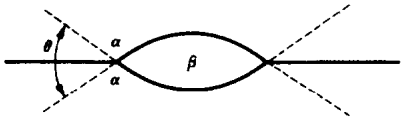

Fig. 1.7. Nucleation of β-phase in an isotropic αα grain boundary.

The ratio of the critical energy of formation of a boundary nucleus ΔG_B^* to that for homogeneous nucleation of a spherical nucleus ΔG_H^* is

$$\Delta G_B^*/\Delta G_H^* = \tfrac{1}{2}(2 - 3\cos\theta + \cos^3\theta). \tag{1.8}$$

Because there are fewer potential sites available for grain-boundary nucleation than for homogeneous nucleation within the grains, the nucleation rate for a grain size d is changed from the homogeneous rate by a factor

$$\frac{\delta}{d}\exp\left(\frac{\Delta G_H^* - \Delta G_B^*}{kT}\right), \tag{1.9}$$

where δ is the grain-boundary thickness. The order of magnitude of the ratio δ/d is typically 10^{-6}, so by substituting this in (1.9), one would expect to observe grain-boundary nucleation being faster than homogeneous nucleation when $\Delta G_H^* - \Delta G_B^* \geqslant 14kT$.

Cahn (1956, 1957) has derived equations for the rates of heterogeneous nucleation at various singularities in a solid. On the basis of incoherent nuclei and isotropic surface tension, he has compared the barriers for nucleation on grain boundaries, corners and edges. Fig. 1.8 illustrates the conditions giving the highest volume nucleation rate for each kind of defect. In the perfect catalysis case (with $\sigma_{\alpha\alpha}/\sigma_{\alpha\beta} = 2$) nucleation can take place without the aid of the activation energy, and the rate of formation of the nucleus is then only determined by the activation energy of grain-boundary diffusion, U_b. From fig. 1.8 it is clear that for substrates of low $\sigma_{\alpha\alpha}/\sigma_{\alpha\beta}$ and high Δg_c, homogeneous nucleation dominates, whereas corners dominate only at the lowest Δg_c.

Observations by field-ion microscopy and by electron microscopy indicate that the structure of a curved boundary surface is not constant, but that imperfections such as ledges and grain-boundary dislocations are present in the interface. It is frequently observed that grain-boundary nucleation occurs only in certain regions of the boundary, e.g. in the case of the precipitation of $(Cr,Fe)_{23}C_6$ from stainless steel where the shape and density of grain-boundary particles vary with the orientation of the boundary. It appears probable therefore, that these heterogeneities of distribution of grain-boundary phases are associated with the presence of singularities in the grain-boundary structure itself.

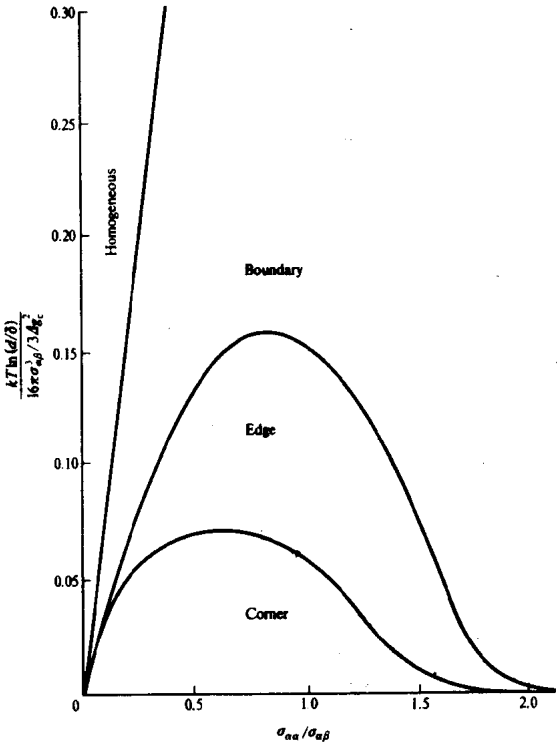

Fig. 1.8. Conditions giving the greatest volume nucleation rates for various kinds of defect. The ordinate represents the opposing factors $kT \ln (d/\delta)$ and the homogeneous nucleation energy, ΔG_H^*. The abscissa represents the catalytic effectiveness of the grain boundaries, with $\sigma_{\alpha\alpha}/\sigma_{\alpha\beta} = 0$ denoting zero catalytic effect (a contact angle of π) and $\sigma_{\alpha\alpha}/\sigma_{\alpha\beta} = 2$ giving perfect catalysis (After Cahn, 1956.)

Nucleation on other planar defects

Fig. 1.9 provides an example which compares the precipitation kinetics of a particular phase (the carbide $(Cr,Fe)_{23}C_6$) in association with various interfaces in an austenitic stainless steel. A family of 'C' curves is shown which represent the time of first appearance of the carbide at a particular site. In comparison with grain-boundary nucleation, it is seen that *twin boundaries* form nuclei at longer times, because of their lower interfacial energy (1.7). In accord with this principle, *coherent twin* interfaces are seen to be more difficult to nucleate upon than *incoherent twin* interfaces. On the other hand, it is seen that $\delta\gamma$-phase boundaries in the matrix are more effective than γ-grain boundaries in promoting carbide nucleation. This is because the energy of $\delta\gamma$-interfaces will be higher than

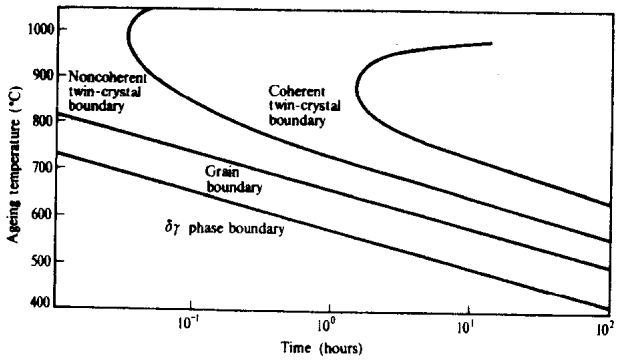

Fig. 1.9. Rate of nucleation of $(Cr, Fe)_{23} C_6$ at different types of interfaces in an austenitic stainless steel. (After Stickler & Vinckier, 1963.)

that of $\gamma\gamma$-boundaries due to a change in composition as well as a change in structure across them.

Superlattice domain boundaries can act in a similar way in suitable systems: for example, in α-Fe–Al alloys there is evidence of domain boundaries catalysing nucleation of precipitates. There is also good evidence of precipitate nucleation at *stacking-faults*. The segregation of solute atoms to pre-existing stacking-faults, first proposed by Suzuki, may lower the stacking-fault energy and thus generate zones within the crystal which differ in structure and composition from the matrix. If a phase can be formed with the same stacking sequence as the fault, then its nucleation will be promoted by the contribution to surface-energy or strain-energy terms in (1.7). The Al–Ag system illustrates this effect well, in that a hexagonal γ′-phase forms on the {111} planes of the fcc matrix.

1.2.3 Strain-energy effects

Lattice misfit between a precipitate nucleus and the matrix can arise from the difference in lattice parameters or the difference in lattice symmetry of the two phases. As illustrated in figs. 1.4*a* and *b*, the misfit can be accommodated by elastic distortions or by defects lying in the interface.

If the unit cell sides of the precipitate and matrix are a_β and a_α respectively, then the misfit between the lattices (δ) is defined as

$$\delta = \frac{2(a_\beta - a_\alpha)}{a_\beta + a_\alpha} \approx \frac{a_\beta - a_\alpha}{a_\beta}. \tag{1.10}$$

In order to calculate g_e, Nabarro (1940) assumed that the nucleus *and* matrix are both strained isotropically, and applied a continuum mechanics

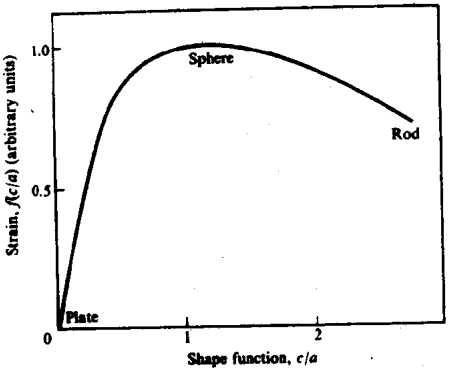

Fig. 1.10. The strain, $f(c/a)$, of an incoherent spheroidal nucleus as a function of its shape: a is the radius and $2c$ the thickness of the spheroid. (After Nabarro, 1940.)

approach to obtain the value of g_e, which was *independent* of the shape of the particle

$$g_e = \frac{6G_\beta\delta^2}{1 + 4G_\beta/3K_\alpha}, \tag{1.11}$$

where G_β is the shear modulus of the precipitate phase and K_α is the bulk modulus of the matrix. If the value of Poisson's ratio is taken as 0.3 then $K = 2G$, so if the moduli of the matrix and precipitate are similar, then

$$g_e \approx 4G\delta^2.$$

For hard particles in a softer matrix, it is more realistic to assume that the nuclei are unstrained, and that only the matrix suffers hydrostatic strain. In this case Nabarro found that g_e becomes a function of the shape of the particle, in that the specific strain-energy decreases in the direction sphere → rod → plate (fig. 1.10).

Plate-shaped nuclei are frequently observed in systems of practical importance. There are factors additional to that of maintaining g_e which favour such a particle shape, namely: (i) the anisotropy of the *surface energy*, so that the habit plane of the plate is that of best crystallographic fit; (ii) The anisotropy of the *elastic constants* of the crystal lattice, so that the habit plane of the plate is perpendicular to the direction of minimum Young's modulus; and (iii) the planes in which dislocations dissociate, or upon which vacancy clusters condense may lead, as already discussed, to the nucleation of plate-like precipitate particles.

In describing the structural relationship between the matrix and a precipitate there are two independent factors which must be considered. Firstly, the *orientation relationship* between the crystal lattices of matrix